A Study on the Mechanical Behavior of butt joint in STS 304L by Hybrid(CO_2 Laser + MIG) Welding

하이브리드 용접에 의한 **STS 304L**

맞대기 용접부의 역학적 거동에 관한 연구

August 2009

Graduate School of Chosun University

Department of Naval Architecture and

Ocean Engineering

Seong Bo-Ram

A Study on the Mechanical Behavior of butt joint in STS 304L by Hybrid(CO_2 Laser + MIG) Welding

Advisor : Professor Han-Sur Bang

A Thesis submitted for the degree of

Master of Engineering

August 2009

Graduate School of Chosun University

Department of Naval Architecture and

Ocean Engineering

Seong Bo-Ram

CONTENTS

List of Figure

List of Table

ABSTRACT

A study on the Mechanical Behavior of butt joint in STS 304L by Hybrid(CO_2 Laser + MIG) Welding

Seong Bo-Ram
Advisor : Prof. Bang Han-Sur Ph.D.
Department of Naval Architecture & Ocean Engineering,
Graduate School of Chosun University

하이브리드 용접은 두 가지 열원을 복합적으로 사용하여 각각의 용접법에 따라 발생하는 단점을 상호 보완하는 용접법으로 타 용접법에 비해 깊은 용입 깊이, 빠른 용접속도와 Arc의 안전성이 우수한 용접법이다. 최근에는 일반적인 용접이 어려운 강종이나, 선박과 같은 후판을 사용하는 대형 구조물 제조 공정에 하이브리드 용접을 적용하기 위한 시도 및 연구가 시행되면서 그 장점이 점점 부각되고 있다.

스테인리스강은 고부가가치 합금으로서 내식성, 내열성 등의 특성이 우수하여 조선, 원자력산업, 화력발전, 보일러, 자동차 부품 등 다양한 분야에서 사용되고 있다. 그러나 스테인리스강에 대한 하이브리드 용접의 적용은 거의 전무한 실정이다.

이에 본 연구에서는 화학 Plant, LNG Tank 등에 사용되고 있는 13mm 두께의 STS 304L에 대하여 하이브리드 용접의 적용 가능성을 검토하기 위해 12kw급 Hybrid(CO_2 Laser +MIG) 시스템을 이용하여 실험을 수행하였다.

실험에 의한 용접공정변수의 최적화를 통해 선정된 가장 우수한 용접 조건에 대하여 유한요소법에 의한 열전도 해석과 열탄소성 해석을 실시하여 하이브리드 용접부의 열적거동(thermal Behavior) 및 잔류응력(residual stress)을 파악하고, X-ray Stress Analyzer를 이용하여 용접부의 잔류응력 값과 수치해석 값을 비교하여 수치해석 결과가 타당함을 입증하였다.

그리고 용접부의 기계적 특성을 고찰하기 위하여 경도(hardness test), 충격(impact test), 인장 실험(tensile test)을 실시하여 강도측면에서 우수한 결과를 얻었고, 최종적으로 STS 304L에 대하여 하이브리드 용접의 적용 가능성을 확인 할 수 있었다.

Chapter 1. Introduction

1.1 Backgrounds & Purposes

Hybrid welding combines two different sources of radiations and offers many advantages compared to conventional welding processes. The main advantages of hybrid welding are reduction of laser power, higher welding speed, increased seam strength, better process stability, less stress fractures, and improved gap bridging.

Just as in the automobile industry, shipbuilders also try to reduce material consumption and weight in order to keep operating costs as low as possible and improve the speed of production. In the last few years, interest in these hybrid processes has risen because of the increasing shipbuilding industrial application of laser welding processes, which have certain limitations. Naturally industry is ever searching for welding techniques offering higher power, higher productivity and a better quality. Therefore it is important to have a details research based on the hybrid laser welding process applied to steel and other materials, and to have the ability both to counsel interested companies and to evaluate the feasibility of implementation of this process. Butt configuration of arc welding of thick plate presently carried out in the ship building industry and their corresponding modification by hybrid welding has been compared in table 1.1

Table 1.1 Compare to Arc & Hybrid welding process in ship building

	Are welding	Hybrid welding
Butt	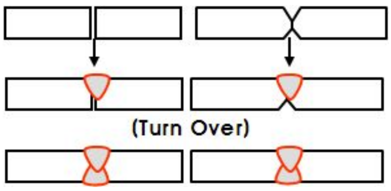	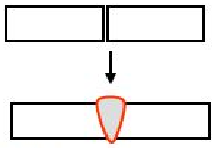 (Delete of turn over)

STS 304L used in this experiment is a kind of STS 304 of low carbon steel. It has almost same corrosion resistance as other stainless steels have, but it keeps a corrosion resistance after welding without a heat treatment because of an outstanding resistance on intergranular corrosion. So, it has been using at LNG TANK, chemical TANK, chemical industry which STS 304 could not bear up against an intergranular corrosion.

New welding technology has been required for improvement of productivity and quality and making up the weak points of conventional welding method and process. Hybrid welding combines two welding methods, laser and arc welding. Advantages of each can be maximized in concurrence with complementing the disadvantages.

In this study, hybrid welding has been carried out on STS 304L, being used under that environment and then carried out advance study with experiment and analysis for application thereafter.

Laser Welding

- Tight fit-up conditions
- Fast welding speed
- Deep penetration
- Low level deformation
- High cost

+

GM / GT / Plasma Welding

- Good bridging ability
- Slow welding speed
- Wide weld seam
- High level deformation
- Low cost

Benefits of Hybrid welding?

- Reduced welding time due to increased travel speed and greater tolerance control
- Low weld distortion – improved fairness
- Tolerant of weld joint fit-up and gaps
- Enhanced weld quality

Fig. 1.1 Benefits of hybrid(laser + arc) welding process

1.2 Scope of Study

A superior structure having excellent safety and economical efficiency can be fabricated, since it become possible to apply high corrosion-resistance and durability of stainless steel into the industrial area. However, as the characteristics showed, the stainless steel should be required to take care of getting proper quality as it is used in extremely severe environment.

The welding defects are easily occurred by material properties and working environment during and after welding, especially the welding residual stress and deformation, occurred by restriction during the partial heating and cooling, deteriorate the brittleness and buckling strength of the welded structures and have bad influence on safety of structures.

Consequently, the researches about the welded structures to be carried out sufficiently in order to estimate and trace the origin of residual stress and deformation in welds precisely and consider the cause prior th welding.

Through analysis of hybrid welded joint, it is to examine the mechanical behavior, caused by hybrid welding and consequently obtain the mechanical properties and stability in welding joint.

In order to achieve these purposes, the analysis of non-stationary heat conduction by finite element method was carried out. The effect of heat source and temperature dependency of physical coefficient(resistivity, heat conduction, specific heat and density and so on) is considered. Also the analysis of heat distribution and welding residual stresses by computing programme is used for numerical analysis which was performed considering the temperature dependency of mechanical properties yield stress, elastic coefficient and heat expansion coefficient and so on). Moreover, the optimum parameters of hybrid welding were determined based on experiments and mechanical testing.

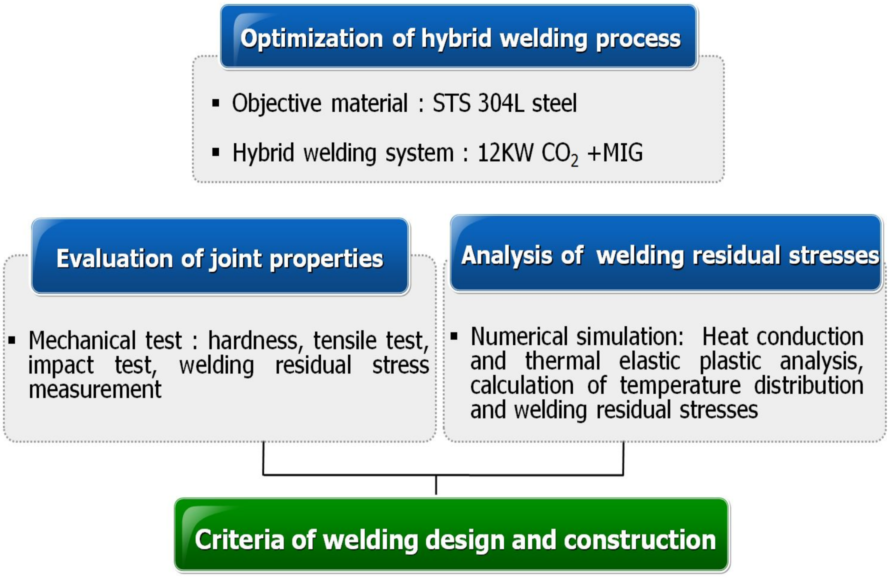

Fig. 1.2 Research objective and method

1.3 Theoretical Basis for Analysis

1.3.1 Heat Conduction Theories

Fourier's law is an empirical law based on observation. It states that the rate of heat flow, dQ/dt, through a homogeneous solid is directly proportional to the area, A of the section at right angles to the direction of heat flow, and to the temperature difference along the path of heat flow, dT/dx i.e.

$$q = -\lambda_x \frac{dT}{dx} \qquad (2.1)$$

So for 2D-case the rate of heat transfer is

$$\frac{\partial}{\partial x}\left(\lambda_x \frac{\partial T}{\partial x}\right) + \frac{\partial}{\partial y}\left(\lambda_y \frac{\partial T}{\partial y}\right) \qquad (2.2)$$

The thermal analysis was conducted using temperature dependent thermal material properties. From conservation of energy the governing equation of heat conduction in weldment is obtained as (considering the medium to be isotropic)

$$\rho c \frac{\partial T}{\partial t} = \lambda\left(\frac{\partial^2 T}{\partial x^2} + \frac{\partial^2 T}{\partial y^2}\right) + \dot{Q} \qquad (2.3)$$

where

T : Temperature (℃)

ρ : Density (g/cm^3)

$\dot{Q}$: Rate of temperature change due to heat generation per volume (cal/cm^3· sec)

t : Time (sec)

λ : Thermal conductivity of isotropic material (cal/cm^3· sec· ℃)

c : Specific heat (cal/g· ℃).

Boundary condition to solve the equation (2.3) is given in the following form using the heat flux q (cal/cm^3· sec· ℃) in normal direction on the boundary of the object.

$$q = -\lambda \frac{\partial T}{\partial n} \qquad (2.4)$$

Heat conduction problem for the object of analysis is formulated as the finite element method using Galerkin method. Internal temperature of the element, T, is given by

$$T(x, y, t) = [N(x, y)]\{\Phi(t)\} \qquad (2.5)$$

where $[N]$ is a shape function matrix shown the relation between nodal temperature and internal temperature of the element. $\{\Phi\}$ is the vector of the nodal temperature of the element at time t.

1.3.2 Thermo-elastic-plastic Theories

A. Basic theory for thermal stress analysis by finite element method

The increment of strain in the element is given by appropriate differentiation of the internal displacements as shown in bellows.

$$\{d\varepsilon\} = [B]\{dw\} \quad (2.6)$$

The increment of stress in element is obtained by using an appropriate matrix $[D]$, the elasticity matrix $[D^e]$ or the plasticity matrix $[D^p]$, and the increment of strain.

$$\{d\sigma\} = [D]\{d\varepsilon\} \quad (2.7)$$

If the increment of initial strain $\{d\varepsilon_0\}$ exists, increment of stress is expressed as follows.

$$\{d\sigma\} = [D]\{d\varepsilon - d\varepsilon_0\} \quad (2.8)$$

where the initial strains are function of temperature such as thermal strains and has the following relation.

$$\{d\varepsilon_0\} = \{d\varepsilon^T\} = \{\alpha\}dT \quad (2.9)$$

Using this relation, the increment of stress, equation (2.8), can be rewritten in the following form.

$$\{d\sigma\} = [D]\{d\varepsilon\} - [C]dT \quad (2.10)$$

The relationship between the increment of the nodal force, $\{dF\}$, and the nodal displacement, $\{dw\}$, is obtained by applying the principle of virtual work as bellows.

$$\begin{aligned}\{dF\} &= \int [B]^T[D]\{d\varepsilon\}dV - \int [B]^T[C]dTdV \\ &\equiv [K]\{dw\} - \{dL\}\end{aligned} \quad (2.11)$$

B. Stress and strain relation dependent upon temperature

1) Stress-strain relation in elastic range

In the elastic range, the increment of total strain consists of increment of elastic strain $\{d\varepsilon^{e}\}$ and the increment of thermal expansion strain $\{d\varepsilon^{T}\}$ as bellows.

$$\{d\varepsilon\} = \{d\varepsilon^{e}\} + \{d\varepsilon^{p}\} \qquad (2.12)$$

The increment of thermal expansion strain is expressed using the coefficient of linear expansion.

$$\{d\varepsilon^{T}\} = \{\alpha\}dT \qquad (2.13)$$

When the elasticity matrix, $[D^{e}]$, changes as temperature increase, the increment of elastic strain is given in the following form.

$$\begin{aligned}\{d\varepsilon^{e}\} &= [D^{e}]^{-1}\{d\sigma\} + \frac{\partial[D^{e}]^{-1}}{\partial T}\{\sigma\}dT \\ &\equiv \{d\varepsilon^{e'}\} + \{d\varepsilon^{T'}\}\end{aligned} \qquad (2.14)$$

2) Stress-strain relation in plastic range

Yield of materials is occurred when its yield function, f, satisfy the following equation.

$$f = 0 \qquad (2.15)$$

According to the associated flow rule (increment theory of plasticity), the increment of plastic strain, $\{d\varepsilon^{p}\}$, is given in following form.

$$\{d\varepsilon^{p}\} = \lambda\left\{\frac{\partial f}{\partial \sigma}\right\} \qquad (2.16)$$

where f is plastic potential and λ is a positive scalar.

Chapter 2. Optimum welding condition by each parameters

2.1 Selection of workpiece

STS 300 series, which has a high strength, outstanding ductility and toughness under low temperature, are Fe-Cr-Ni alloy steel that are suitable to apply for structures under an extremely low temperature.

STS 304L used in this experiment is a kind of STS 304 of low carbon steel, it has almost same corrosion resistance as much as others have, but it keeps a corrosion resistance after welding without a heat treatment because of an outstanding resistance on intergranular corrosion. So, it has been using at LNG tank, chemical tank, chemical industry which STS 304 could not bear up against an intergranular corrosion. Table1.1 & Table 1.2 shows chemical compositions and Mechanical Properties of STS 304L.

Table 2.1 Chemical compositions of STS 304L (%)

Grade	C	Mn	Si	P	S	Ni	Cr
STS304L	0.022	1.748	0.379	0.028	0.026	8.12	18.2

Table 2.2 Mechanical Properties of STS 304L

Grade	Yield.S (N/mm^2)	Tens. S (N/mm^2)	Charpy Impact	Elongation(%)	Hardness (Vickers)
STS304L	245	550	216J	40	200

2.2 Fabrication of workpiece

Fig. 2.1 is configuration of welded specimen laser + MIG by hybrid welding with a length 600mm, width 500mm and thickness 13mm. Experimental set-up for CO_2 Laser + MIG hybrid welding is shown Fig 2.2.

Considering various parameters, butt joint of STS 304L by laser + MIG hybrid welding were carried out. For the experiment, 12kw CO_2 laser was used together with conventional welding equipment consisting of a welding mode 500A, Fronius TPS 5000. The MIG torch was connected close to the laser focusing optic at an angle of about 45°. Shielding gas was supplied through a MIG torch located at the side of laser head (Arc leading).

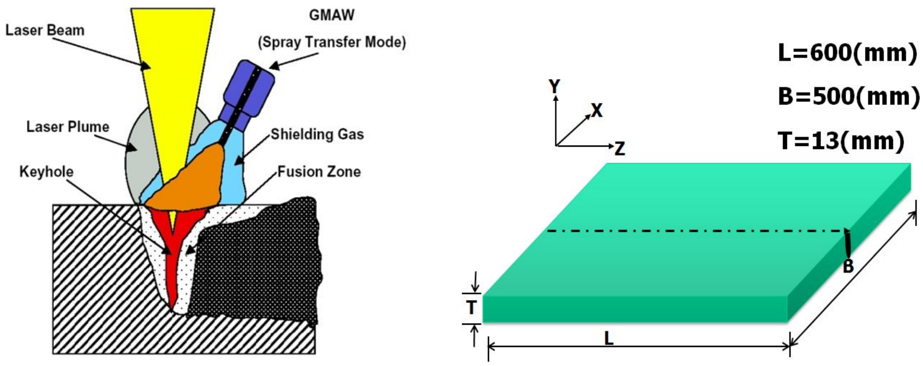

Fig. 2.1 Configuration of welded specimen and coordinate

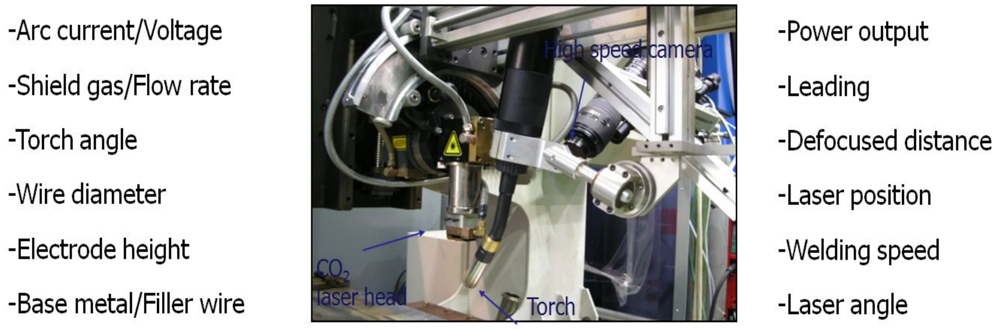

Fig. 2.2 Experimental set-up for CO_2 Laser + MIG hybrid welding

2.3 Shielding gas, power of Laser and Mig, welding speed etc

The employed welding conditions for fabrication are shown in Table 2.3. The surface of primer was cleaned by brush. The employed welding conditions for Laser + MIG hybrid welding are shown in Table 2.3. Determined optimum welding conditions is shown in Table 2.4. The hybrid weldment is constructed by the full-penetration welding.

The predominant constituent of the shield gas is generally an inert gas such as helium or argon. A shield gas providing a higher ionization potential is required since the plasma can deflect or absorb a portion of the laser energy when CO_2 lasers are employed. Helium is therefore often preferred to argon for laser welding, but its lightness is a disadvantage and it is often combined with argon which is heavier without substantial alteration of the weld penetration depth. The addition of reactive gases such as oxygen and carbon dioxide has been shown to have an influence on the weld pool wetting characteristics and bead smoothness.

From Fig 2.4, it is clear that shield gas of full penetration has been obtained. Fig 2.5 is the top and bottom bead shapes according to hybrid welding condition.

Table 2.3 Employed welding condition of hybrid welding

Item		welding condition
CO_2 Laser Power(KW)		10,11,12
MIG	Wire Type/ Diameter	KS D7026 Y308 / 1.2mm
	Voltage (V)	21~29
	Current (A)	220~300
	CTWD (mm)	20
	Wire feeding speed(m/min)	9.8
Welding Speed (cm/min)		100~150
Interspace (mm)		4
Gap (mm)		0
Shielding gas		He60~70%, Ar28~32%, $CO_2$3~10%

Welding condition	Top bead	Back bead
12kw, 26V, 300A, 1m/min He70%, Ar30%, $CO_2$0%	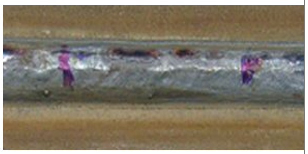	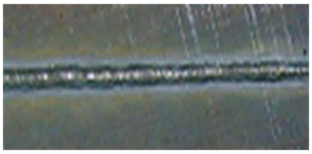
12kw, 27V, 300A, 1m/min He70%, Ar25%, $CO_2$5%		
12kw, 26V, 300A, 1m/min He70%, Ar28%, $CO_2$2%	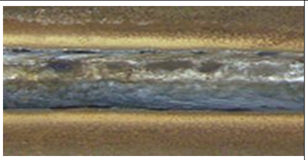	
12kw, 27V, 300A, 1m/min He65%, Ar32%, $CO_2$3%		

Fig. 2.3 Bead surfaces of bead on plate welds by hybrid welding

(a) 12kw, 29V, 300A, 1m/min (He70%, Ar25%, $CO_2$5%)

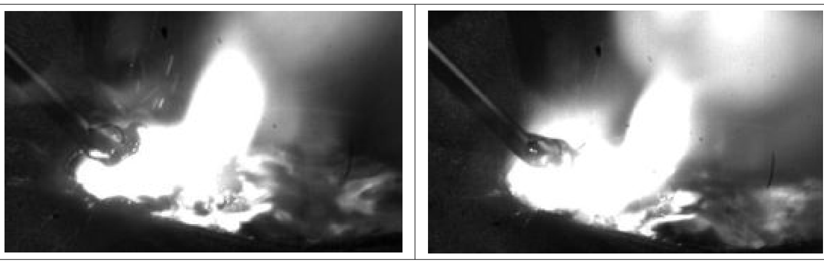

(b) 12kw, 29V, 300A, 1m/min (He70%, Ar22%, $CO_2$8%)

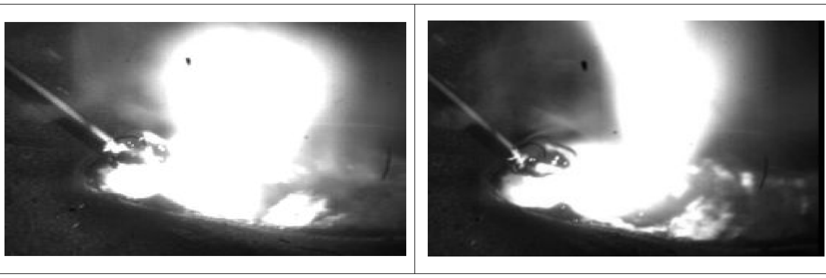

(c) 12kw, 27V, 300A, 1.3m/min (He65%, Ar28%, $CO_2$7%)

(d) 12kw, 27V, 300A, 1.3m/min (He65%, Ar32%, $CO_2$3%)

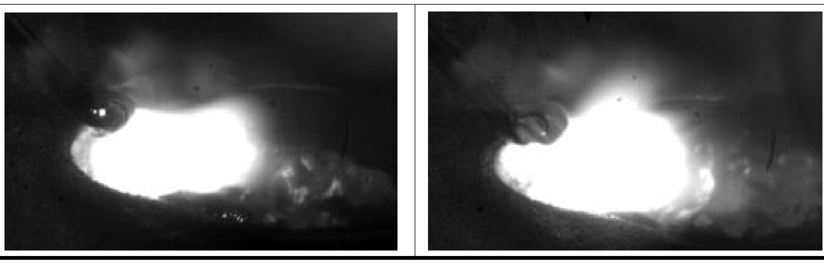

Fig. 2.4 High speed image of hybrid welding condition

Welding condition	Top bead	Back bead
(a) 12kw, 29V, 300A, 0.8m/min He70%, Ar22%, $CO_2$8%		
(b) 12kw, 29V, 300A, 1m/min He70%, Ar25%, $CO_2$5%	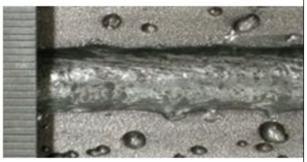	
(c) 12kw, 29V, 300A, 1m/min He65%, Ar28%, $CO_2$7%		
(d) 12kw, 27V, 300A, 1.3m/min He65%, Ar32%, $CO_2$3%		

Fig. 2.5 Bead surfaces of butt joint by hybrid welding

Table 2.4 Optimum welding condition of hybrid welding

Item		Optimum welding condition
CO_2 Laser Power(KW)		12
MIG	Wire Type/ Diameter	KS D7026 Y308 / 1.2mm
	Voltage (V)	27
	Current (A)	300
	CTWD (mm)	20
	Wire feeding speed(m/min)	9.8
Welding Speed (cm/min)		130
Interspace (mm)		4
Gap (mm)		0
Shielding gas		He65%, Ar32%, $CO_2$3%

Chapter 3. Welding heat distribution in weldment

During the welding, the weldment is subjected to complex thermal cycles by welding heat source, so then, the residual stresses, metallurgical change and distortion are caused by thermal effect in workpiece. In order to reduce these problem, it is necessary first to predict the temperature distribution that develops in the weldment.

This chapter discusses the heat distribution in SAW and hybrid weldment using the Finite Element Analysis.

3.1 Simulation condition

In other for accurate analysis of the heat distribution in weldments, the following conditions are taken into consideration.

1) Two dimensional un-steady state heat distribution analysis is conducted using 4-node iso-parametric element
2) The thermal coefficient of material varies with the temperature and the thermal condition is treated as non-linear function
3) The thermal conduction to the inside of material and the thermal transfer to the air are treated as a thermal boundary condition
4) The material is iso-tropic media, so that its properties at each point are the same along all directions and the initial temperature is 20℃
5) The recovery temperature of mechanical stiffness in material is assumed, 750℃

Fig. 3.1 shows the thermal coefficient of stainless steel, considered for welding heat distribution simulation.

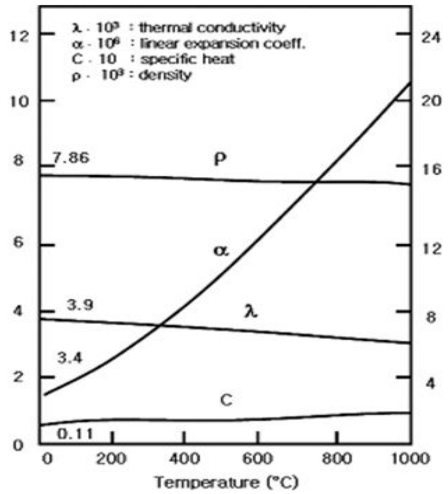

Fig. 3.1 Thermal coefficient of stainless steel

3.2 Boundary condition

The boundary condition employed for the thermal elastic-plastic analysis is illustrated in Fig 3.2. The one end of specimen is fixed and other area is free to expand and contract along the width-direction(X) and the thickness-direction(Y).

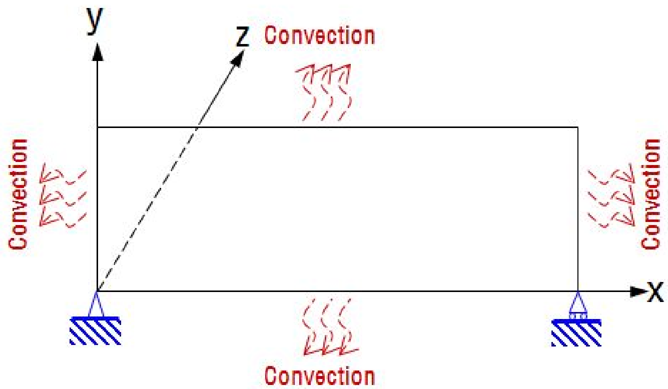

Fig. 3.2 Boundary conditions for elastic-plastic analysis

3.3 Finite Element Model for Hybrid welding

The welding heat source for analysis can be sorted out non-split type and split type as shown in Fig. 3.3 Non-split type has uniform flux (CASE.1) and split type is divided into volume to volume heat source (CASE.2) and volume to surface heat source (CASE.3). In this study CASE.2 was selected for analysis because it was proved that CASE.2 is proper method for heat source analysis of laser arc hybrid welding. Fig. 3.4 is schematic diagram of heat source.

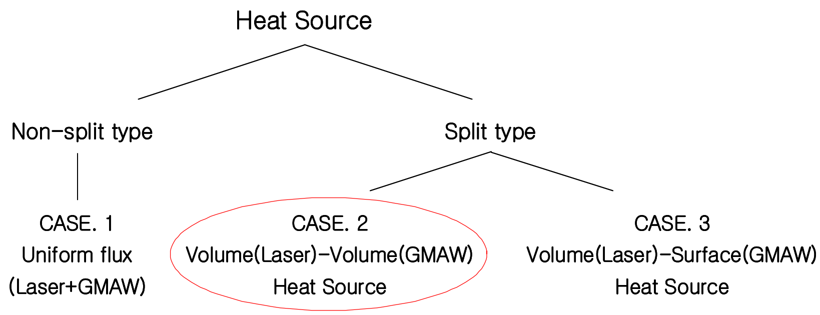

Fig. 3.3 Heat sources for analysis

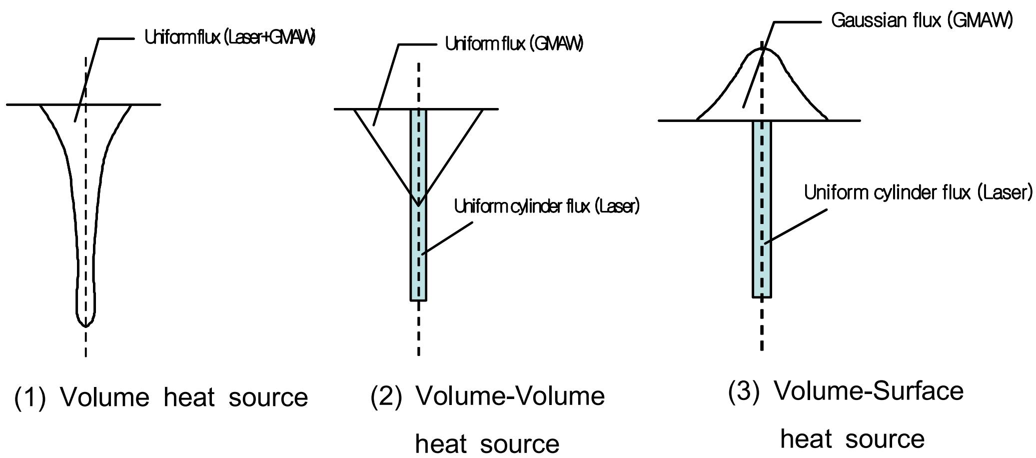

Fig. 3.4 Schematic diagram of heat source

As shown in Fig. 3.5 the meshed model consists of 2114 nodes and 1950 elements, and the elements are partitioned into $1 \times 1 mm^2$ in welds and getting bigger and wider as the distance from the welds increases considering the welding heat effect to weldment. That is, the welds and the region near the welds is affected severely by the welding heat and the thermal effect decreases as the distance from the welds increase.

In order to observe cross section, welded specimen has been cut by wire cutting grinded and polished by sandpaper, then has carried out etching with $CuSO_4$ 10mg +HCl 50mg + H_2O 50mg.

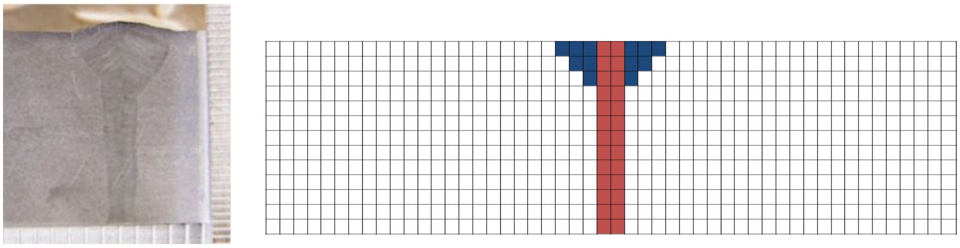

Fig. 3.5 Finite element model of heat source in hybrid welding

3.4 Calculation of heat input

To compare with hybrid welding, we have simulated with submerged arc welding(SAW) conditions which actually being used when welded on 13mm stainless steel.

3.4.1 SAW weldment

From the equation(3.1), the heat input, Q, is determined and welding arc efficiency is 80%. the equation(3.1) shows that the amount of heat supplied to the welds, Q, is proportional to the welding current and arc voltage but decreases with increase of welding speed.

$$Q = \eta_A \frac{VI}{W_S} \tag{3.1}$$

where Q : Heat input

η_A : Efficiency of arc welding

V : Arc Voltage (V)

I : Arc Current (A)

W_S : Welding speed (cm/sec)

In addicion, Heat flux to each element is determined from the equation (3.2) considering the welding condition and the size of weld metal.

$$q = \frac{Q \cdot \ell}{4.19 \cdot A \cdot \ell \cdot t} \tag{3.2}$$

where, t : Time (sec)

ℓ : Welding length (mm)

Q : Heat input (J/cm)

A : Unit area (mm^2)

Table 3.1 Welding conditions for simulation in SAW

	Pass	Current(A)	Arc voltage(V)	Welding speed (cm/min)
Welding Conditions	before	840A	38V	61
	after	900A	38V	61

3.4.2 Hybrid weldment

A. Mig welding

Heat input equation used in numerical simulation of Mig welding is same in SAW.

Table 3.2 Welding conditions for simulation in Mig welding

	Current(A)	Arc voltage(V)	Welding speed (cm/min)	Efficiency of arc welding (η_A)
Welding Conditions	300A	26.9V	130	80%

B. CO_2 Laser welding

The heat input, Q, is determined by the following equation(3.3) and proportional to the beam power but decreases with the increase of welding speed.

$$Q = \eta_L \frac{P}{W_S} \tag{3.3}$$

where η_L : Efficiency of laser welding

P : Laser power (kW)

W_S : Welding speed (cm/sec)

Simulation conditions for CO_2 laser are shown in Table 3.3. Efficiency of CO_2 laser welding fixed 60% which was calculated considering total absorption and losses of laser beam.

Table 3.3 Welding conditions for simulation in CO_2 laser

Welding Conditions	Laser power (kW)	Welding speed (cm/min)	Efficiency of CO_2 laser welding (η_L)
	12kW	130	60%

3.5 Simulation for welding heat distribution in weldments

3.5.1 SAW weldment

Since the SAW weldment is constructed by 2pass welding, the temperature distribute in different location at each passage as shown Fig. 3.6. From those phenomenons, it can be seen that the temperature spreads uniformly to the region near the welds because the material is isotropic media.

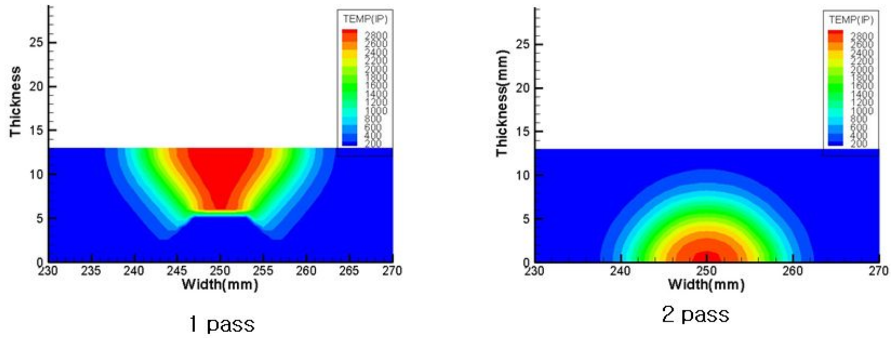

Fig. 3.6 Temperature contour in SAW

3.5.2 Hybrid weldment

Fig 3.7 shows the temperature distribution phenomenon by CO_2 laser+Mig hybrid welding in hybrid weldment. The welding heat source penetrates the welds and conducts to the workpiece along the width-direction of weldment as a line heat source does.

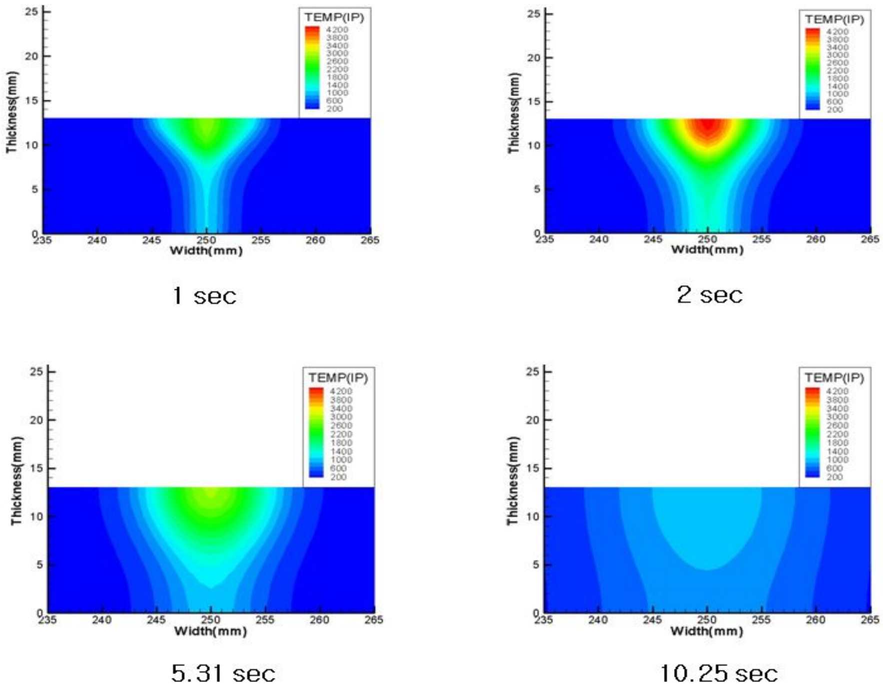

Fig. 3.7 Temperature contour in hybrid welding

3.5.3 Thermal history curve

Fig. 3.8 and Fig. 3.9 describe the temperature increase and cooling rate in both weld metal, heat affected zone and base metal as a function of temperature and time.

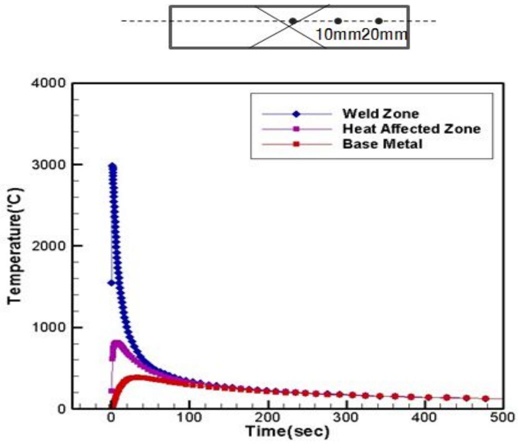

Fig. 3.8 Thermal history in SAW welding

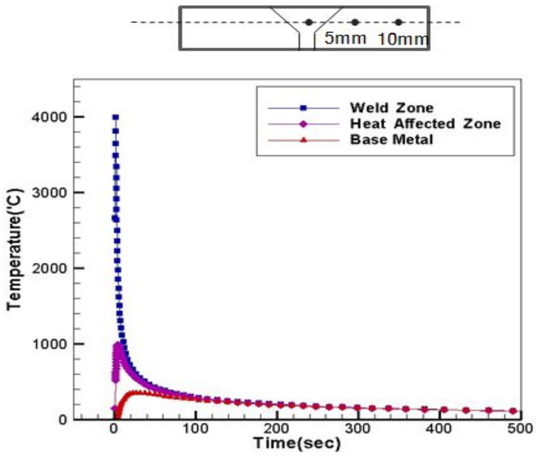

Fig. 3.9 Thermal history in hybrid welding

When examining the thermal history curves between SAW and hybrid welds, the local temperature in both welds reaches the melting point instantaneously and fall off rapidly, so then, the welds is highly restrained by the adjacent area during freezing and cooling.

It can be assumed that the heat generated by welding heat source in hybrid weldment dissipates at a faster rate to the area near the welds and in the SAW weldment, the area affected by welding heat source is wider than that in hybrid weldment, so then, the hardened area is wider in SAW weldment.

Chapter 4. Welding residual stress distribution in weldments

During the welding, the weldments is heated locally by the welding and undergoes temperature change that causes the complex strains and non-elastic strain in weld metal and the base metal mear the welds. After the welding is completed, the residual stresses caused by strains remains in weldment.

This Chapter discusses the welding residual stresses caused by welding in SAW and hybrid weldments, especially, the important stresses, such as the longitudinal stresses, acting paralled to the direction of the weld bead, and the transverse stresses, acting vertical to the direction of the weld bead, are mainly discussed.

4.1 Simulation condition

In other to analyze the welding residual stresses in SAW and hybrid weldments using the thermal elasto-plastic numerical simulation program, the following conditions are adopted, and the resulting data obtained from the heat distribution analysis is used as the input data.

1) The temperature dependency of mechanical properties (yield stress, young's modulus, thermal expansion coefficient) of stainless steel are considered
2) The solid is isotropic media
3) The plane deformation(plane stress, plane strain) is assumed in weldment for the two-dimensional thermal elasto-plastic analysis
4) The input data for the numerical simulation is obtained from the welding heat distribution analysis
5) The size and distribution of welding heat source are treated as thermal load
6) The phase transformation effects is not considered in the present analysis

Fig. 4.1 shows the Mechanical properties of stainless steel considered during thermal elasto-plastic analysis.

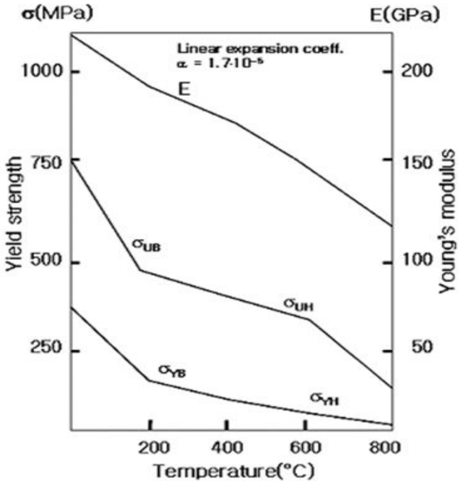

Fig. 4.1 Mechanical properties of stainless steel

4.2 Elastic-plastic analysis in SAW weldment

The Finite Element Model for the elastic-plastic analysis is the same model adopted for heat distribution analysis in Chapter 3. Since the residual stress develops and its pattern changes with a weld pass, it is analysis considering the stresses.

Fig. 4.2 shows the final welding residual stress distribution in the upper part(Y=12mm) of SAW weldment. In regard to the longitudinal stress(sigma Z), the high tensile stress occur in the welds and in the vicinity of welds, and transfer to the compressive stress as the distance increase from the center of weld bead. The high magnitude of stresses in the welds is 50 kgf/mm^2. In case of the transverse stresses(sigma X), the tensile stress occurs in welds, turn to the compressive stress in the region near the welds and remains the compressive stress in the base metal of weldment. But magnitude of stress is almost zero in welds.

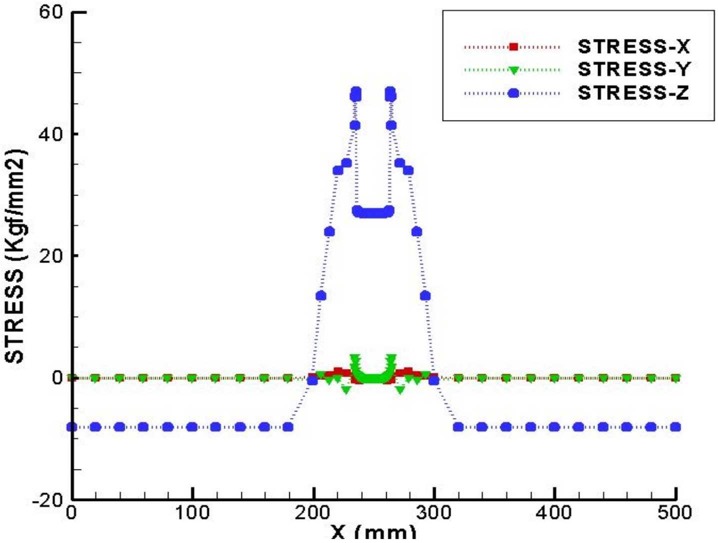

Fig. 4.2 Numerical results of residual stress in SAW

4.3 Elastic-plastic analysis in hybrid weldment

The Finite Element Model for the elastic-plastic analysis is the same model adopted for heat distribution analysis in Chapter 3. Fig. 4.3 shows the distribution pattern of the welding residual stresses in the upper (Y=12mm), middle (Y=6mm), and lower part (Y=1mm) of hybrid weldment.

The tensile longitudinal stress (sigma Z) are caused in welds and distribute symmetrically in all region. The highest magnitude of stress at the upper, middle and lower part of the weldment is 44 kgf/mm^2, 47 kgf/mm^2 and 42 kgf/mm^2.

The compressive transverse stress (sigma X) develops in welds of the upper and lower part of weldment and turns to the tensile component in the vicinity of the welds. But the tensile stress occur in the middle part and transfer to the compressive stress in the region near the welds.

The magnitude of stresses in the middle part are higher than that in other region, it is considered that this region cools slowly in comparison with the upper and lower part and is restrained by the upper and lower part of weldment. The numerical residual stress of hybrid welding is slightly less than SAW. This also means that arc welding makes more deformation than hybrid welding.

Fig. 4.4 is shows comparison of welding residual stress by FEM analysis and measurement. The analyzed residual stresses and the measured residual stresses distribute in similar manner. But the analyzed stresses is higher than the measured residual stresses.

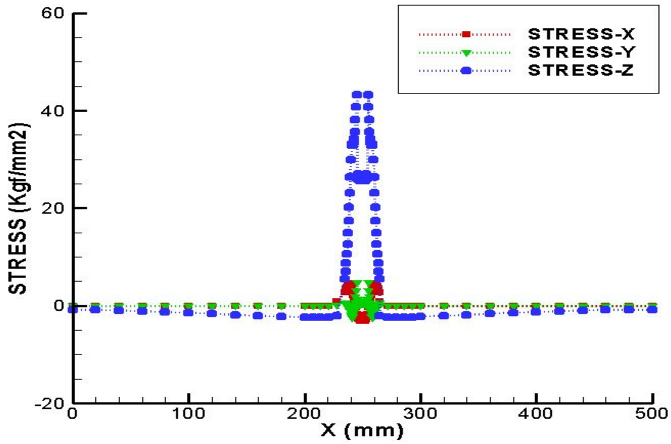

(a) Distribution of stress in the upper part of weldment (Y=12mm)

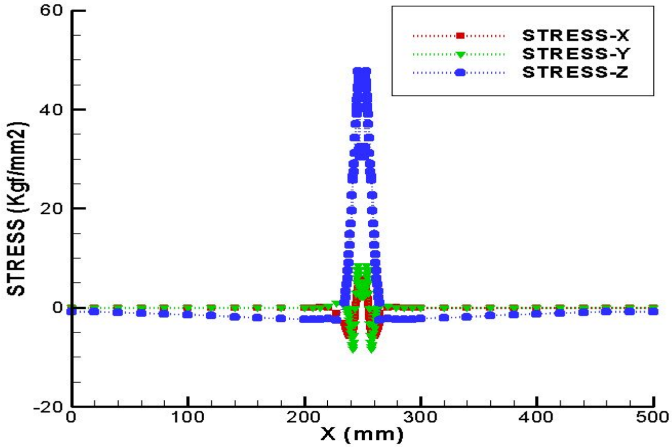

(b) Distribution of stress in the middle part of weldment (Y=6mm)

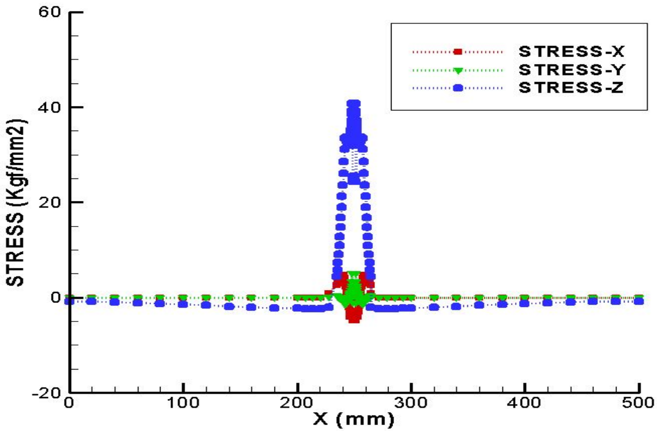

(c) Distribution of stress in the lower part of weldment (Y=1mm)

Fig. 4.3 Numerical results of residual stress in hybrid welding

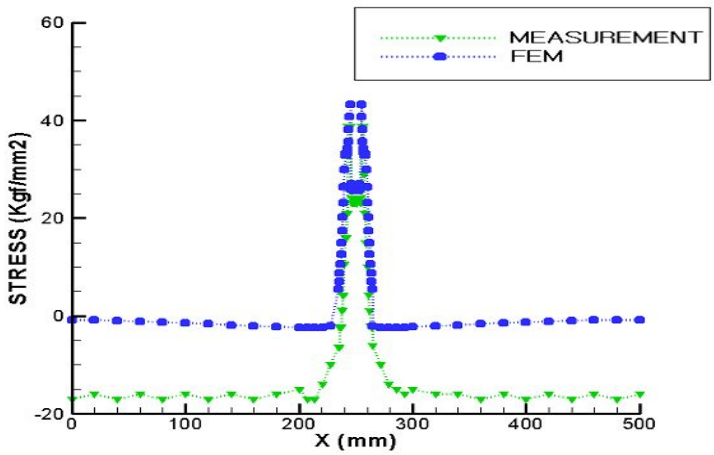

Distribution of stress in the upper part of weldment (Y=12mm)

Fig. 4.4 Comparison of welding residual stress by FEM analysis & measurement

Chapter 5. Mechanical Characteristics of Hybrid welds

5.1 Hardness Test

A Hardness test has been carried out with Vickers Hardness Test Machine, shown in Fig. 5.1. and a micro hardness measurement was made on transverse sections of each weldments. A load of 1kg and a spacing of 0.5mm between the indentations were used in 1 mm, 10 mm below of top surface. Measured values of each welds are shown Fig. 5.2.

As shown in Fig. 5.2, the hardness have the similar magnitude in weld metal, base metal, HAZ. The hardness of STS 304L was between 170~200 Hv.

Fig. 5.1 Vickers Hardness Test Machine

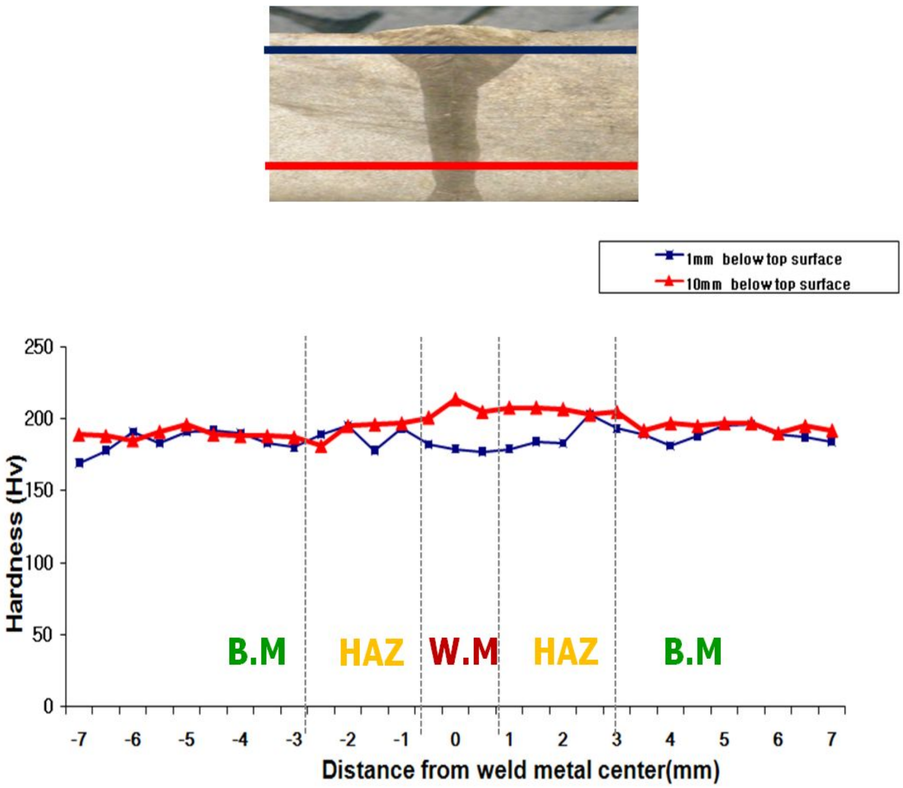

Fig. 5.2 Hardness values for hybrid welded specimen

5.2 Tensile test

Tensile tests provide information on the strength and ductility of welded materials under uni-axial tensile stress. The pertinent data obtained from a tension test is ultimate tensile strength, yield strength, percent elongation, and the stress-strain relationship. Fig 6.6 shows the tensile testing machine and the dimensions of the test specimens based on ASTM standards. Fig 5.4 show the tensile tested specimens of hybrid butt joint and stress-strain graph obtained from the experiment. The result of the yield strength is 670 MPa.

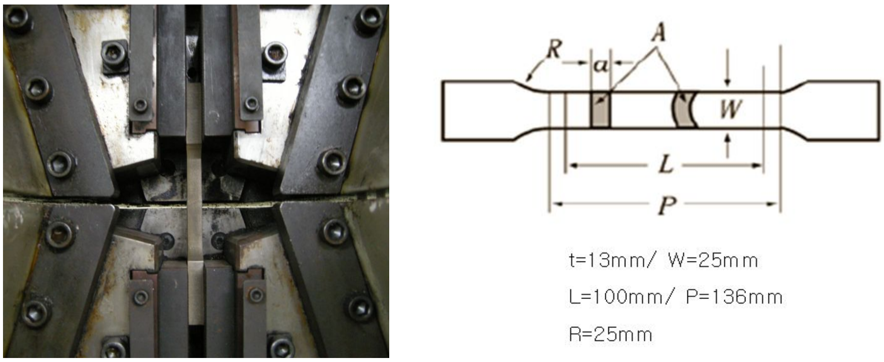

Fig. 5.3 tensile test machine & Dimension of tensile test specimen

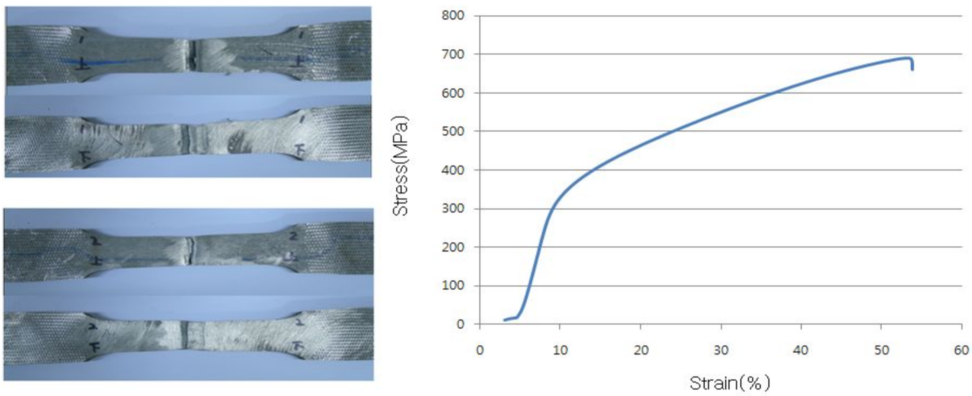

Fig. 5.4 Tensile test specimens of butt joint and its stress-strain graph

5.3 Impact Test

The Charpy test provides a measure of the energy required to break a material under impact loading. The test consists essentially of a hammer with a given amount of energy striking a notched test piece of fixed dimensions and recording the energy required to fracture the test piece at a specific temperature and recording whether the fracture mode was ductile or brittle.

Fig 5.5 shows the Charpy test machine and the KS standard specimen dimension for impact testing. The Charpy specimen has a square cross section (10 x 10 mm) and contains a 45˚ V notch, 2 mm deep with a 0.25 mm root radius. The specimen is supported as a beam in a horizontal position and loaded behind the notch by the impact of a heavy swinging pendulum. The specimen is forced to bend and fracture at a high strain rate on the order of $10^3 s^{-1}$.

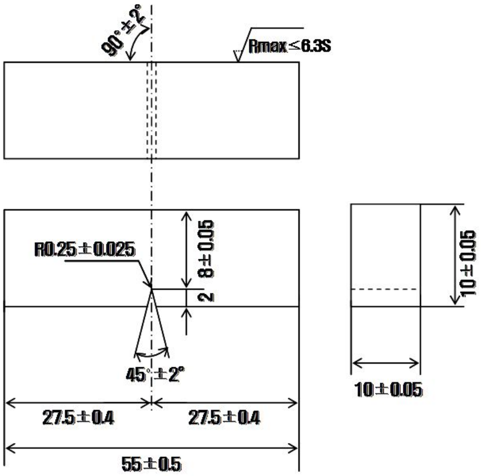

Fig. 5.5 Impact test machine & Dimension of Charpy Impact test specimen (KS 0821)

Fig 5.6 shows the impact tested specimens of the hybrid welding. Table 5.1 is the tabulated result showing the comparison of the impact test results for hybrid welding in the weld zone.

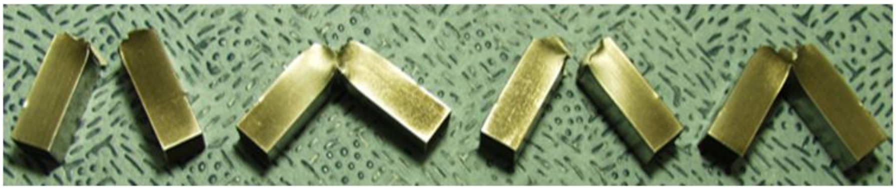

1 2 3 4

Fig. 5.6 Impact tested specimens of hybrid welding

Table 5.1 Result of impact test

	Temperature	Angel	Result	Standard
1	0℃	145˚	143.08J	Min. 150J
2	-20℃	145˚	284.20J	
3	0℃	150˚	164.64J	
4	-20℃	150˚	282.24J	

Chapter 6. Conclusion

In this study, thermal behavior and mechanical characteristics of laser + MIG hybrid welding in STS 304L was investigated. And the application in industrial fields has been justified.

From this study, the following conclusions can be drawn:

1) As a result of this study, optimum welding condition was determined by experiments. The optimum welding conditions were as follows: laser power 12kw, arc current 300A, arc voltage 27V, welding speed 130cm/min and He65%, Ar32%, $CO_2$3% of shielding gas composition. Also these conditions were obtained in arc leading case. And if the laser power is higher than 12kW, the speed could be further increased.

2) Heat transfer and temperature history could be predicted by numerical simulation using FEM. Combination heat source model of split type (volume by MIG and volume by CO_2 laser) has been considered to analyze the heat source of hybrid welding.

3) Thermal history with temperature gradient has been obtained from the numerical simulation results. This phenomena can be explained by laser welding which has a higher cooling time compared to arc welding.

4) The numerical residual stress of hybrid welding is slightly less than SAW. This also means that arc welding makes more deformation than hybrid welding. And the middle part of hybrid weldment cools at the slow rate and is restrained by the upper and lower part, the maximum value of stress develops at the

middle part of welds.

5) From the result of welding residual stress measurement, when comparing the measured and analyzed result, same pattern of residual stresses distribution has been observed and the analyzed results are slightly higher.

6) From the result of tensile test, it has been observed that the fracture is generated at base metal, slightly away from HAZ in all specimens. But the strength appears higher than that of the base metal.

7) From the result of hardness test, weldment have the similar magnitude of hardness in weld metal, the base metal, HAZ.

8) Thus a preliminary study on the hybrid welding application in STS 304L has been successfully carried out.

Reference

1. J. Tusek and M. Suban. "Hybrid welding with arc and laser beam."Science and Technology of Welding and Joining, Vol.4, No.5 pp.308-311, 1999

2. Klas Nilsson, Hans Engstrom, Alexander Kaplan. "Influence of Butt-and T-joint preparation in Laser Arc Hybrid Welding." International Institute of Welding, IIW-Doc. XII 1732-02, pp.273-284, Copenhagen 2002.

3. S. G. Hong and J. B. Lee. "Effect of laser and arc power on the penetration depth in CO2 laser-MIG hybrid welding."Proceedings of Korean Welding Society, pp.81-83. May 2003. (in Korean)

4. STAUFER HERBERT. "Laser-Hybrid Welding of Ships."Welding Journal pp.39~43, American Welding Society, June 2004.

5. Young-Pyo Kim, "The Study on Mechanical Behavior of Butt Joints in Al-Mg Alloys by Hybrid(CW Nd:YAG Laser+MIG) Welding", Ph.D. Thesis, Chosun University, Korea, February. 2005

6. C M Allen, Laser welding of aluminum alloys – principles and applications, The Welding Institute REPORT, March 2004.4. H.S. Bang and Y.P. Kim. “Fundamental Study on The Heat Input Model of Hybrid Welding for The Finite Element Analysis.” Proceedings of the 2003 Autumn Annual Meeting of Korean Welding Society, pp.36~38, 2003. (in Korean)

7. Yukio Ueda, You Chul Kim, Teruhisa Yamakita and Han Sur Bang. “Applicability of Substituting Plane-deformation Problems for Three-dimensional Thermal Elasto-plastic Problems.” Journal of Japan Welding Society. Vol.6, No.1, pp.47~53,1988.

8. H.S. Bang and Y.C. Kim. “Analysis on The Three-Dimensional Unstationary Heat Conduction on The Welding of Thick Plates by F.E.M.” Journal of the Korean Welding Society, Vol.9, No.2, pp.37~43, Jun 1991.

9. H.S. Bang. “Study on The Mechanical Behaviour of Welded part in thick Plate - Three-dimensional Thermal Elasto-Plastic Analysis Base on Finite

Element Method." Journal of the Korean Welding Society, Vol.10, No.4, pp.37~43, December 1992.

10. H.S. Bang and Y.P. Kim. "Fundamental Study on The Heat Input Model of Hybrid Welding for The Finite Element Analysis". Proceeding of the 2003 Autumn Annual Meeting of Korean Welding Society, pp.36~38, 2003.(In Korea)

11. J. Tusek and M. Suban. "Hybrid welding with arc and laser beam."Science and Technology of Welding and Joining, Vol.4, No.5 pp.308-311, 1999

12. Hans Engstrom, Klas Nilsson, Jan Flinkfeldt, Tony Nilsson, Anders Skirfors, Bertil Gustavsson. "Laser Hybrid Welding of High Strength Steels." Proc. of the Laser Materials Processing Conference ICALEO'01, Oct. 15-18, Jacksonville, FL, USA. 2001

13. Ulrich Dilthey. "Laser Arc Hybrid Welding an Overview." International Institute of Welding, IIW-Doc. XII 1710-02, pp.243-248, Copenhagen 2002.

14. Klas Nilsson, Hans Engstrom, Alexander Kaplan. "Influence of Butt- and T-joint preparation in Laser Arc Hybrid Welding." International Institute of Welding, IIW-Doc. XII 1732-02, pp.273-284, Copenhagen 2002.

15. S. G. Hong and J. B. Lee. "Effect of laser and arc power on the penetration depth in CO2 laser-MIG hybrid welding."Proceedings of Korean Welding Society, pp.81-83. May 2003. (in Korean)

16. STAUFER HERBERT. "Laser-Hybrid Welding of Ships."Welding Journal pp.39~43, American Welding Society, June 2004.

17. H. Staufer. "Laser-GMA welding, a new joining technology." Technical articles, Fronius International Gmbh (www.fronius.at)

18. Hyung-Shik Kim. "Study on the laser Hybrid Welding Technology for Shipbuilding." Journal of KWS, Vol. 22, No. 2, pp.19~22, April 2004. (in Korean)